

Curvature-Driven Morphing of Non-Euclidean Shells

Matteo Pezzulla^a, Norbert Stoop^b, Xin Jiang^a, Douglas P. Holmes^a

^a*Department of Mechanical Engineering, Boston University, Boston, MA, 02215*

^b*Department of Mathematics, Massachusetts Institute of Technology - Cambridge, MA, 02139*

Abstract

We investigate how thin structures change their shape in response to non-mechanical stimuli that can be interpreted as variations in the structure's natural curvature. Starting from the theory of non-Euclidean plates and shells, we derive an effective model that reduces a three-dimensional stimulus to the natural fundamental forms of the mid-surface of the structure, incorporating expansion, or growth, in the thickness. Then, we apply the model to a variety of thin bodies, from flat plates to spherical shells, obtaining excellent agreement between theory and numerics. We show how cylinders and cones can either bend more or unroll, and eventually snap and rotate. We also study the nearly-isometric deformations of a spherical shell and describe how this shape change is ruled by the geometry of a spindle. As the derived results stem from a purely geometrical model, they are general and scalable.

Keywords: Swelling, Curvature, Shells, Geometry, Morphing

1. Introduction

Non-mechanical stimuli, such as temperature, pH, and swelling have significant influences on the shape of a structure. The bending of bimetal thermostats is perhaps the first rationalized example of how temperature can induce shape changes (Timoshenko, 1925). Under a homogeneous temperature change, the two metal layers in the bimetal expand different amounts, causing differential stresses that result in bending with uniform curvature. The swelling of gels, elastomers, and foams can cause a significant increase in their volume (Hong et al., 2008; Lucantonio et al., 2013), and if swelling causes different parts of a material to expand more in response to the same amount of solvent, nontrivial shape changes can occur (Klein et al., 2007; Holmes et al., 2011; Kim et al., 2012). The physics behind thermal expansion and swelling are rather different from each other, yet the resulting shape changes can sometimes be qualitatively and quantitatively similar, highlighting the underlying geometric connection of these non-mechanical stimuli to local volume changes in the material. If the structure is thin, even small volume changes can have dramatic consequences on an object's shape. These large, geometrically nonlinear deformations are ever present in the growth and reconfiguration of thin biological structures. For instance, the contraction of the spherical, fluid-filled shell of a *Volvox* embryo turns itself inside out to enable motility (Höhn et al., 2015), while the differential drying of a pollen grain causes it to morph into a spindle to slow dessication (Katifori et al., 2010). Differential growth rates in the plane of a growing leaf will cause it to develop wrinkles along its edge (Boudaoud, 2010). These morphogenetic shapes have analogues with completely mechanical systems as well, where pre-stretch can play the role of growth. Although swelling may develop in a variety of ways, it is usually convenient to identify two main categories, which are in-plane or through-the-thickness differential swelling. When swelling develops within the mid-surface of the body, flat plates can buckle into hyperbolic surfaces (Klein et al., 2011; Pezzulla et al., 2015) or bend into domes (Kim et al., 2012), and when swelling develops across the thickness, plates can deform into cylinders (Pezzulla et al., 2016).

Email addresses: pezzulla@bu.edu (Matteo Pezzulla), stoopn@mit.edu (Norbert Stoop), ssjiang@bu.edu (Xin Jiang), dpholmes@bu.edu (Douglas P. Holmes)

The modeling of growth in three-dimensional elasticity has led to the so-called *incompatible elasticity*, which began with the introduction of the multiplicative decomposition of the deformation gradient in Kondurov and Nikitin (1987), borrowed from models in plasticity. Since thin structures can undergo small stretching strains as a consequence of their slenderness (Rayleigh, 1894), scientists developed reduced ordered models in complete analogy to what has been done in standard mechanics for the theory of plates and shells (Love, 1888; von Kármán, 1910; Koiter and Simmonds, 1973). In particular, a theory for the growth of plates and shells in the context of incompatible elasticity, named theory of non-Euclidean plates and shells, was presented in Efrati et al. (2009) and successfully applied in Armon et al. (2011); Pezzulla et al. (2015, 2016), just to name a few. A refined geometric theory of morphoelastic shells was also recently derived in Sadik et al. (2016). The large deformability of thin structures offers a pathway towards the design of smart systems that can completely change their shape (Py et al., 2007), while at times taking advantage of elastic instabilities (Amar and Goriely, 2005; Goriely and Ben Amar, 2005). This connection between differential expansion, or growth, to thin, naturally curved structures motivates the study of how shells deform in response to variations in their natural curvature.

In this paper, we investigate the shape changes that can be induced on plates and shells when a non-mechanical stimulus acts through-the-thickness. Starting from the theory of non-Euclidean plates and shells, we derive nonlinear geometric models that show the influence of the initial curvature on the shape change, from flat plates to spherical shells. As the non-mechanical stimulus is enclosed in the concept of natural curvature (Audoly and Pomeau, 2010), the derived models are general, purely geometrical and, as such, scalable. The paper is organized as follows. In Section 2, we set the notation and provide a brief summary of the theory of non-Euclidean plates and shells. In Section 3, we present a straightforward procedure to derive the expressions of the natural forms when a general plate or a shell is subjected to a stimulus that can be represented by a variation in its natural curvatures. We show how the resulting natural curvature can be seen as the sum of a homothety of the initial shape plus a spherical shape-changing natural curvature. In Section 4, we apply the general method presented in the previous section to intrinsically flat shells such as plates, cylinders, and cones. When the shape is extrinsically curved, we also show how growth can trigger snap-through instabilities, and provide a simple formula for the stability threshold in terms of the natural curvature. Finally, in Section 5, we study the effects of variations in natural curvature of spherical shells, providing a proof for the method presented in Section 3 through a comparison of 3D and 2D numerical results. Moreover, we show how this shape change is similar to the one developed by pollen grains during harmomegathy (Katifori et al., 2010), and show how these shapes are similar to spindles.

2. General considerations

We identify a shell with its mid-surface $\mathcal{S} \subset \mathcal{E}$, where \mathcal{E} is the three-dimensional Euclidean space provided with a cartesian basis $(\mathbf{e}_1, \mathbf{e}_2, \mathbf{e}_3)$ as shown in Figure 1. The shell, viewed as a three-dimensional body, is a bounded domain $\mathcal{B} \subset \mathcal{E}$, such that $\mathcal{B} = \mathcal{S} \times [-h/2, h/2]$, where h is its thickness. The body can be naturally endowed with a system of curvilinear coordinates chosen in reference to the embedding of the initial configuration $\hat{\mathbf{r}}(\eta^1, \eta^2, \eta^3): \mathcal{D} \rightarrow \mathcal{E}$, where we choose (η^1, η^2) so that they span the mid-surface of the shell while η^3 runs along the normal $\hat{\mathbf{n}}$ to the mid-surface, and \mathcal{D} represents the domain of parametrization of the reference configuration. In the following, we will denote with \mathbf{r} the embedding of the deformed configuration, and with \mathbf{n} the normal to the deformed mid-surface. Not only does the parametrization of the initial configuration endow the body with a system of coordinates, but it also provides it with a three-dimensional metric $\hat{\mathbf{g}}$ and a covariant basis $(\hat{\mathbf{g}}_1, \hat{\mathbf{g}}_2, \hat{\mathbf{g}}_3)$. The covariant metric coefficients of the reference configuration are defined as $\hat{g}_{ij} = \hat{\mathbf{r}}_{,i} \cdot \hat{\mathbf{r}}_{,j}$, where commas denote partial derivatives, Latin indices run from 1 to 3, and the symbol \cdot denotes the standard inner product in the Euclidean space. When one deals with standard compatible elasticity, meaning that no inelastic stimuli act on the body, the metric $\hat{\mathbf{g}}$ is the base state for the measurement of strains. However, when the body is subjected to some inelastic stimuli such as growth or swelling, the strain is measured with respect to a relaxed, natural metric $\bar{\mathbf{g}}$, modeling the rest lengths induced by the stimulus (Amar and Goriely, 2005; Nardinocchi and Teresi, 2007; Efrati et al., 2009). While the metric $\hat{\mathbf{g}}$ is derived from the embedding $\hat{\mathbf{r}}$, the natural metric $\bar{\mathbf{g}}$ is formulated *ad hoc* for the specific stimulus at hand. As a result, the metric $\bar{\mathbf{g}}$ trivially corresponds to a null Riemann curvature tensor

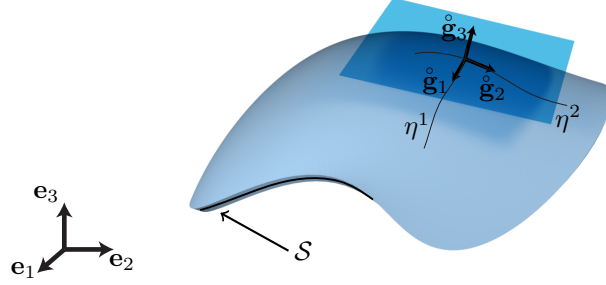


Figure 1: A shell in its reference state embedded in the Euclidean space. The tangent coordinates (η^1, η^2) are shown as well as the covariant base vectors.

while the natural metric $\bar{\mathbf{g}}$ may not, in general, and cannot be embedded in the Euclidean space (O'Neill, 1997). Moreover, we denote with $g_{ij} = \mathbf{r}_{,i} \cdot \mathbf{r}_{,j}$ the covariant metric coefficients of the deformed configuration. Finally, as the time scales associated with growth or swelling are much larger than those associated with inertia, we neglect inertia loads and, in general, the following analyses hold for quasi-static stimuli.

Since reduced order models are based on the geometry of the mid-surface, we briefly recall some concepts from differential geometry following O'Neill (1997). The first fundamental form $\mathring{\mathbf{a}}$ of a surface parametrized by $\mathring{\mathbf{R}} = \mathring{\mathbf{r}}|_{\eta^3=0}$ has covariant components $\mathring{a}_{\alpha\beta} = \mathring{\mathbf{R}}_{,\alpha} \cdot \mathring{\mathbf{R}}_{,\beta}$ while the second fundamental form $\mathring{\mathbf{b}}$ has covariant components $\mathring{b}_{\alpha\beta} = \mathring{\mathbf{n}} \cdot \mathring{\mathbf{R}}_{,\alpha\beta}$ (Greek indices run from 1 to 2). The eigenvalues of the second fundamental form are the principal curvatures of the surface: the average of the eigenvalues is called mean curvature H , and their product is the Gaussian curvature K . Probably the most important theorem in differential geometry, Gauss's Theorema Egregium, states that the Gaussian curvature is an isometric invariant. Finally, we denote with $a_{\alpha\beta} = \mathbf{R}_{,\alpha} \cdot \mathbf{R}_{,\beta}$ and $b_{\alpha\beta} = \mathbf{n} \cdot \mathbf{R}_{,\alpha\beta}$, the first and second fundamental forms of the deformed mid-surface, respectively. The theory of non-Euclidean plates or shells (Efrati et al., 2009; Armon et al., 2011) is derived from three-dimensional incompatible elasticity, based on the Kirchhoff assumptions, resulting in a dimensionless elastic energy that is usually written as

$$\bar{\mathcal{U}} = \int_{\omega} [(1-\nu)\text{tr}(\mathbf{a} - \bar{\mathbf{a}})^2 + \nu \text{tr}^2(\mathbf{a} - \bar{\mathbf{a}})] d\omega + \frac{h^2}{3} \int_{\omega} [(1-\nu)\text{tr}(\mathbf{b} - \bar{\mathbf{b}})^2 + \nu \text{tr}^2(\mathbf{b} - \bar{\mathbf{b}})] d\omega, \quad (1)$$

where ν is the Poisson ratio, tr denotes the trace operator in the surface metric defined by $\bar{\mathbf{a}}$, $d\omega$ is the relaxed area element $d\omega = \sqrt{\det \bar{\mathbf{a}}} d\eta^1 d\eta^2$, \mathbf{a} is the first fundamental form of the mid-surface, containing all information about lateral distances between points, and \mathbf{b} is the second fundamental form of the mid-surface, containing all information about the local curvature. The natural first and second fundamental forms $\bar{\mathbf{a}}$ and $\bar{\mathbf{b}}$ represent the lateral distances and curvatures that would make the sheet locally stress-free, and they are determined by the specific stimulus. As forms of a surface embedded in Euclidean space, \mathbf{a} and \mathbf{b} must satisfy the Gauss-Codazzi-Mainardi equations (O'Neill, 1997), while the natural forms $\bar{\mathbf{a}}$ and $\bar{\mathbf{b}}$ do not have the same constraints, and can be incompatible. This is analogous to the lack of a three-dimensional compatibility requirement on $\bar{\mathbf{g}}$, which could be not embeddable in the Euclidean space, differently from \mathbf{g} . It is this incompatibility, in addition to that imposed by geometric confinement when present, which drives the deformation of the shell.

As a stimulus is intrinsically three-dimensional, the natural metric $\bar{\mathbf{g}}$ that describes it has to be consistently reduced to the first and second natural fundamental forms $\bar{\mathbf{a}}$ and $\bar{\mathbf{b}}$ of the mid-surface. One example of the dimensional reduction of a three-dimensional natural metric into first and second natural fundamental forms was nicely presented in Armon et al. (2011). In that case, two flat sheets were pre-stretched by different amounts in different directions and then glued on top of each other. The pre-stretch of the sheet is viewed as an in-plane conformal stretch of the three-dimensional reference metric of each sheet, neglecting the Poisson effect along the thickness. If the two sheets are pre-stretched differently (in magnitude and/or

direction), the natural metric of the bilayer sheet is discontinuous. When a metric discontinuity is encountered along the mid-surface of the sheet, it cannot be approximated as continuous, and bending energy will smooth out the discontinuity in the realized, visible metric as well documented in Moshe et al. (2013), and shown in Pezzulla et al. (2015). However, when the discontinuity develops across the thickness of the sheet, *i.e.* the smallest length of the body, the natural metric may be approximated as a continuous linear function of η^3 (Armon et al., 2011). This approximation is consistent with the theory of plates and shells, as the three-dimensional visible metric is expanded linearly along the thickness (Koiter and Simmonds, 1973; Ciarlet, 2000; Efrati et al., 2009). This approach was successfully applied in (Armon et al., 2011; Pezzulla et al., 2016) where the discontinuous natural three-dimensional metric was translated into natural first and second fundamental forms. In both papers, only initially flat sheets were considered, neglecting the influence on initial curvature. Moreover, Armon et al. (2011) only considers imposing natural curvature changes without imposing conformal stretching of the mid-surface. In this paper, we present a formal derivation of the first and second natural fundamental forms in the general case of natural stretch and curvature of an initially curved bilayer sheet, where the two layers increase or decrease their local volumes by different amounts. We also show that the model has to be modified to take into account a growth along the thickness, as the absence of which would result in unphysical outcomes in certain cases.

3. Natural forms of shells

As explained in Efrati et al. (2009), the dimensional reduction that leads to the theory of non-Euclidean plates is based on two assumptions: Kirchhoff-Love kinematics and a plane-stress condition. The authors note that the two assumptions stand in contradiction with each other as they represent two different elastic problems – plane-strain versus plane-stress. Therefore, the two do not commute, and the order in which the two assumptions are applied is crucial (Lewicka, 2011). The theory is derived by assuming Kirchhoff-Love kinematics first, followed by applying a plane state of stress assumption. The Kirchhoff-Love assumption can be stated as $\varepsilon_{i3} = 0$, where $2\varepsilon_{ij} = g_{ij} - \bar{g}_{ij}$ is the strain defined as the difference between the visible and the natural metric. On the other hand, if \mathbf{S} and \mathbf{T} denote the first Piola-Kirchhoff and Cauchy stress tensors, respectively, the plane stress condition may be stated equivalently either as $\mathbf{S}\mathbf{n} = \mathbf{0}$ or $\mathbf{T}\mathbf{n} = \mathbf{0}$. The kinematical assumption sets a constraint on the growth along the thickness. For example, in Efrati et al. (2009), the stimulus is assumed to be planar, *i.e.* tangent to the mid-surface at each point, thus not inducing a change of the rest length along the thickness. This is usually stated as $\bar{g}_{i3} = \delta_{i3}$ that implies, through the Kirchhoff-Love assumption, $g_{i3} = \delta_{i3}$. As swelling is an intrinsic spherical stimulus, we relax this assumption and let the rest length along the thickness to vary by an amount Λ_o so that $\bar{g}_{i3} = \Lambda_o^2 \delta_{i3}$. Here, the Kirchhoff-Love assumption implies $g_{i3} = \Lambda_o^2 \delta_{i3}$. This means that the three-dimensional metric can be expanded through the thickness up to the first order as $\mathbf{g} = \mathbf{a} - 2\eta^3 |\mathbf{r}_{,3}| \mathbf{b}$. By recognizing that $|\mathbf{r}_{,3}| = \sqrt{g_{33}} = \Lambda_o$, the expansion reads

$$\mathbf{g} = \mathbf{a} - 2\eta^3 \Lambda_o \mathbf{b}, \quad (2)$$

where the first and second fundamental forms can be computed as

$$\mathbf{a} = \mathbf{g}|_{\eta^3=0}, \quad \mathbf{b} = -\frac{1}{2} \bar{g}^{33} \frac{\partial \mathbf{g}}{\partial \eta^3} \Big|_{\eta^3=0} = -\frac{1}{2\Lambda_o} \frac{\partial \mathbf{g}}{\partial \eta^3} \Big|_{\eta^3=0}. \quad (3)$$

The expansion resulting in equation (2) differs from the one presented in Efrati et al. (2009) by the factor $\sqrt{g_{33}} = \Lambda_o$ that multiplies the thickness coordinate η^3 as also shown in Efrati et al. (2010)¹. This results from the variation in length along the thickness, which is here taken into account. Let us also note that the expansion (2) leads to a slightly different expression of the energy of the non-Euclidean shell:

$$\bar{U} = \int_{\omega} [(1 - \nu) \text{tr}(\mathbf{a} - \bar{\mathbf{a}})^2 + \nu \text{tr}^2(\mathbf{a} - \bar{\mathbf{a}})] d\omega + \Lambda_o^2 \frac{h^2}{3} \int_{\omega} [(1 - \nu) \text{tr}(\mathbf{b} - \bar{\mathbf{b}})^2 + \nu \text{tr}^2(\mathbf{b} - \bar{\mathbf{b}})] d\omega, \quad (4)$$

¹We are not aware of a published version of this paper other than an electronic version at the link provided in the bibliography.

which takes into account the growth of the thickness; note the emergence of the Λ_o^2 term that multiplies the bending energy. We recall that this model is suitable for the description of the large displacement but small strain deformations of a shell. When large strains are involved, dimensional reduction should be carried out by starting from other hyperelastic models, such as Mooney-Rivlin or Neo-Hooke (Lucantonio et al., 2016).

Let us now consider a bilayer shell with initial, geometric first and second fundamental forms $\mathring{\mathbf{a}}$ and $\mathring{\mathbf{b}}$ (figure 1). We assume that the outer layer is locally swelling by a factor α^2 whereas the inner layer is locally swelling by a factor β^2 , meaning that the local volumes would like to change by α^6 and β^6 in the outer and inner layer, respectively. Rest lengths and volumes can be identified by the three-dimensional natural metric within each layer as $\bar{\mathbf{g}} = \alpha^2 \mathring{\mathbf{g}}$ and $\bar{\mathbf{g}} = \beta^2 \mathring{\mathbf{g}}$ in the outer and inner layer, respectively. Within the theory of shells, it is consistent to approximate this discontinuous reference metric as linear within the thickness of the body. If $\eta^3 = 0$ is the equation of the mid-surface of the shell, we generalize the expression used in Armon et al. (2011) to curved surfaces as

$$\bar{\mathbf{g}}(\eta^i) = \alpha^2 \frac{\eta^3 + h/2}{h} \mathring{\mathbf{g}}(\eta^i) - \beta^2 \frac{\eta^3 - h/2}{h} \mathring{\mathbf{g}}(\eta^i). \quad (5)$$

Now, the crucial step is determining the natural first and second fundamental forms induced on the mid-surface by the three-dimensional reference metric. By using (3) for the natural metric we find:

$$\bar{\mathbf{a}} = \bar{\mathbf{g}}|_{\eta^3=0} = \frac{\alpha^2 + \beta^2}{2} \mathring{\mathbf{g}}(\eta^1, \eta^2, 0) =: \Lambda_o^2 \mathring{\mathbf{a}}(\eta^\alpha), \quad (6)$$

$$\bar{\mathbf{b}} = -\frac{1}{2} \bar{g}^{33} \frac{\partial \bar{\mathbf{g}}}{\partial \eta^3} \Big|_{\eta^3=0} = \Lambda_o \mathring{\mathbf{b}}(\eta^\alpha) - \frac{\alpha^2 - \beta^2}{2\Lambda_o h} \mathring{\mathbf{a}}(\eta^\alpha). \quad (7)$$

Before proceeding further, notice that in the case of homogenous stimulus (heating, swelling, etc), $\alpha = \beta$ and the second addend in the expression of the natural second fundamental form is equal to zero, meaning that there is no differential swelling and the shell will just increase its dimensions homothetically as we will discuss later in more detail.

An important concept related to the natural forms is that of natural curvature (Audoly and Pomeau, 2010), since it has a direct and visible meaning: it is the curvature of a beam cut out of the shell. Being a one-dimensional object, the beam is able to adopt the natural curvature that alludes the shell due to constraints placed on the geometry of surfaces. In general, the natural curvature varies with the direction of the cut and the point in which it is evaluated. Let us recall that the principal curvatures κ_δ of a surface with first fundamental form \mathbf{a} and second fundamental form \mathbf{b} can be computed by solving the eigenvalue problem $\det(\mathbf{b} - \kappa_\delta \mathbf{a}) = 0$. Although $\bar{\mathbf{a}}$ and $\bar{\mathbf{b}}$ may be incompatible, *i.e.* they do not satisfy the Gauss-Codazzi-Mainardi equations, and therefore they are not the fundamental forms of a surface in the physical Euclidean space, they correspond to a natural surface embedded in a curved space. Therefore, the principal natural curvatures $\bar{\kappa}_\delta$ may be computed by solving the eigenvalue problem

$$\det(\bar{\mathbf{b}} - \bar{\kappa}_\delta \bar{\mathbf{a}}) = 0. \quad (8)$$

Since we can write equation (7) in mixed coordinates as

$$\bar{b}_\alpha^\gamma = \frac{1}{\Lambda_o} \mathring{b}_\alpha^\gamma - \frac{\alpha^2 - \beta^2}{2\Lambda_o^3 h} \delta_\alpha^\gamma, \quad (9)$$

equation (8) implies

$$\bar{\kappa}_\delta = \frac{\mathring{\kappa}_\delta}{\Lambda_o} - \frac{\alpha^2 - \beta^2}{2\Lambda_o^3 h}. \quad (10)$$

where $\mathring{\kappa}_\delta$ are the principal curvatures of the mid-surface in the reference configuration. As $\bar{b}_{\alpha\beta} = \bar{b}_\alpha^\gamma \bar{a}_{\gamma\beta}$, the second natural fundamental form can be written in terms of the first natural fundamental form and natural curvatures. Notice that differential swelling (or residual swelling, heating, etc) is additive to the initial geometric curvature except for the prefactor $1/\Lambda_o$, which is fundamental for the description of homotheties.

This also means that if a straight bilayer beam bends and achieves a curvature $\bar{\kappa}$, a beam that has an initial curvature $1/R$ and the same thickness structure will simply achieve a final curvature $1/(\Lambda_o R) + \bar{\kappa}$, where we posed $\bar{\kappa} = (\alpha^2 - \beta^2)/2\Lambda_o^3 h$. As regards residual swelling (Pezzulla et al., 2015), $\Lambda_o \simeq 1$ and so the additive decomposition of curvatures becomes even more evident.

While this formalism explains how the stimulus affects the natural forms through the notion of natural curvature, equation (10) cannot be used for a quantitative prediction of the natural curvature as explained in Armon et al. (2011); Pezzulla et al. (2016), due to the arbitrary criterion selected for the choice of the linear approximating reference metric. To wit, let us consider the case of a plate (Armon et al., 2011; Pezzulla et al., 2016), so that $\mathring{\mathbf{b}} = \mathbf{0}$ and $\mathring{\mathbf{a}} = \mathbf{I}$. Equation (10) simply predicts that the natural curvatures would be equal to

$$\bar{\kappa}_\delta = -\frac{\alpha^2 - \beta^2}{2\Lambda_o^3 h}, \quad (11)$$

which is a rather simple formula compared to Timoshenko's one for the bending of bimetallic strips (Timoshenko, 1925) and to the formula for the bending of bilayered gel beams (Lucantonio et al., 2014). Indeed, it stems from a strong approximation that does not minimize the elastic energy, and cannot be used for the prediction of the natural curvature that has to be either measured experimentally (Armon et al., 2011; Pezzulla et al., 2016) or via the formulae presented in Timoshenko (1925); Lucantonio et al. (2014).

3.1. Homogenous heating or swelling of a spherical shell

The problem of the homogeneous heating or swelling of a spherical shell is a clear example in which one has to take into account the change of the rest length along the thickness of the shell, which would otherwise be constrained to grow only along the mid-surface keeping its radius constant. The homogenous growth takes place at zero elastic cost, meaning that both stretching and bending energies are zero. As this requires the natural forms to be compatible, it is interesting to investigate under which conditions the natural forms derived in this section can be compatible in the case of a spherical shell. So, let us write the Gauss-Codazzi-Mainardi equations for orthogonal natural forms:

$$\begin{aligned} \bar{b}_{11,2} &= \bar{b}_{11}\bar{\Gamma}_{12}^1 - \bar{b}_{22}\bar{\Gamma}_{11}^2, \\ -\bar{b}_{22,1} &= \bar{b}_{11}\bar{\Gamma}_{22}^1 - \bar{b}_{22}\bar{\Gamma}_{12}^2, \\ \bar{K} &= -\frac{1}{\sqrt{\bar{a}_{11}\bar{a}_{22}}} \left[\left(\frac{(\sqrt{\bar{a}_{22}})_{,1}}{\sqrt{\bar{a}_{11}}} \right)_{,1} + \left(\frac{(\sqrt{\bar{a}_{11}})_{,2}}{\sqrt{\bar{a}_{22}}} \right)_{,2} \right], \end{aligned} \quad (12)$$

where $\bar{\Gamma}_{\alpha\beta}^\delta$ denotes the Christoffel symbol of the second kind associated with the metric $\bar{\mathbf{a}}$. The first two equations are the Codazzi-Mainardi equations, which represent a structural condition on the second derivatives of the Gauss map, while the last equation represents Gauss's Theorema Egregium for orthogonal metrics (O'Neill, 1997). For the problem at hand, $\bar{\mathbf{a}} = \Lambda_o^2 \mathring{\mathbf{a}}$ and $\bar{\mathbf{b}} = \Lambda_o \mathring{\mathbf{b}}$, where $\mathring{\mathbf{a}}$ and $\mathring{\mathbf{b}}$ are the first and second fundamental form of the undeformed mid-surface of the shell. Since $\mathring{\mathbf{a}}$ and $\mathring{\mathbf{b}}$ satisfy the Gauss-Codazzi-Mainardi equations by definition, we easily see that also the scalar multiples $\bar{\mathbf{a}}$ and $\bar{\mathbf{b}}$ do. Therefore, the natural forms are compatible and homogenous swelling or growth can take place at zero elastic cost. As a result, a spherical shell of radius R will grow to a spherical shell of radius $\Lambda_o R$. If growth along the thickness was not accounted for, the radius would be constrained to stay constant, being the growth limited to the tangent space.

Let us now consider the more general case of differential swelling of a spherical shell of radius R . In this case, equations (6) and (7) can be written as $\bar{\mathbf{a}} = \Lambda_o^2 \mathring{\mathbf{a}}$ and $\bar{\mathbf{b}} = \kappa_o \mathring{\mathbf{b}}$. Substituting these expressions in equations (12), we find that the Codazzi-Mainardi equations are still satisfied while the Gauss equation is verified if and only if $\kappa_o = 1/(\Lambda_o R)$, so only in the homogenous swelling case. When growth is triggered by variations in natural curvature and conformal stretch of the mid-surface, we can then conclude that incompatibility arises only from the Gauss's Theorema Egregium.

4. Intrinsically flat shells

To test this model on differential swelling or growth, we start with the bilayer growth of intrinsically flat shells such as plates, cylinders and cones. Eventually, we will show how plates and cylinders can be recovered as particular cones.

4.1. Plates

The case of plates in which one layer swells relative to the other was largely studied in Pezzulla et al. (2016), where the main result was that incompressible plates eventually bend into cylindrical shapes whose mean curvature is three-fourths the natural curvature divided by the square of the conformal stretch factor $H = (3/4)\kappa_o/\Lambda_o^2$. This result stemmed from first and second natural fundamental forms written as $\bar{\mathbf{a}} = \Lambda_o^2 \mathbf{I}$ and $\bar{\mathbf{b}} = \kappa_o \mathbf{I}$, while their correct expressions were derived in the previous section as (for the case of plates) $\bar{\mathbf{a}} = \Lambda_o^2 \mathbf{I}$ and $\bar{\mathbf{b}} = \kappa_o \Lambda_o^2 \mathbf{I}$. This results in a formula for the mean curvature that does not depend on the conformal stretch factor, namely

$$H = \frac{3}{4}\kappa_o. \quad (13)$$

While this does not affect the results presented in (Pezzulla et al., 2016) as $\Lambda_o \simeq 1$ in that case, it can have large effects for high swelling ratios. We will recover the case of flat plates from that of cylinders presented in the next section.

4.2. Cylinders

Let us consider an open bilayer cylindrical shell of radius R in which one layer shrinks and the other layer swells. If the swelling layer is on the outer part of the cylinder, the shell will increase its curvature; on the contrary, if the inner layer swells, the cylinder will unroll and eventually snap-through, and bend along a direction orthogonal to the initial one, similar to snap bracelets (Kebadze et al., 2004). As the shell is thin, it will try to minimize its stretching energy as much as possible so that in the isometric limit it will be exactly equal to zero. For finite thicknesses, the deformation will slightly deviate from the isometric limit due to the presence of boundary layers of width $\sqrt{h/\bar{\kappa}}$. For a cylinder with cylindrical coordinates $(\eta^1, \eta^2) = (\theta, z)$ we have:

$$\bar{a}_{\alpha\beta} = \Lambda_o^2 \bar{a}_{\alpha\beta} = \Lambda_o^2 \begin{pmatrix} R^2 & 0 \\ 0 & 1 \end{pmatrix}, \quad \bar{b}_{\alpha}^{\eta} = \begin{pmatrix} \frac{1}{\Lambda_o R} + \bar{\kappa} & 0 \\ 0 & \bar{\kappa} \end{pmatrix}, \quad (14)$$

where $\bar{\kappa}$ is the portion of the natural curvature induced by differential swelling.

To determine the shape of the cylinder that corresponds to a particular value of the natural curvature, we minimize the bending energy given by the second addend in equation (4) under the isometric constraint (Pezzulla et al., 2016). We emphasize that for a flat homogeneous metric, as in the case of a cylinder, the Gauss-Codazzi-Mainardi equations admit homogenous second fundamental forms as solutions. Consequently, when minimizing the bending energy, one can minimize the energy density augmented by the constraint on the null Gaussian curvature through a Lagrange multiplier.

The Euler-Lagrange equations associated with the bending energy in (4) are

$$\begin{aligned} 2\left[b_1^1 - \left(\frac{1}{R} + \bar{\kappa}\right)\right] + 2\nu(b_2^2 - \bar{\kappa}) - \lambda b_2^2 &= 0, \\ 2(b_2^2 - \bar{\kappa}) + 2\nu\left[b_1^1 - \left(\frac{1}{R} + \bar{\kappa}\right)\right] - \lambda b_1^1 &= 0, \end{aligned}$$

where λ is the Lagrange multiplier associated with the constraint on the Gaussian curvature. The equations admit the two solutions:

$$\begin{aligned} b_1^1 &= \frac{1}{R} + (1 + \nu)\bar{\kappa}, \quad b_2^2 = 0, \quad \text{with} \quad \bar{U}_b^1 = (1 - \nu^2)(1 + \bar{\kappa}R)^2, \\ b_1^1 &= 0, \quad b_2^2 = \frac{\nu}{R} + (1 + \nu)\bar{\kappa}, \quad \text{with} \quad \bar{U}_b^2 = (1 - \nu^2)\bar{\kappa}^2 R^2. \end{aligned} \quad (15)$$

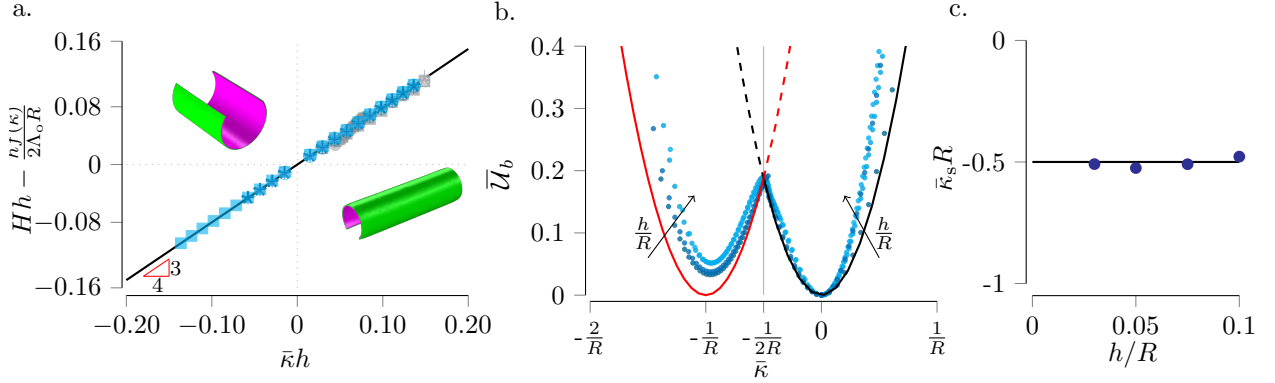


Figure 2: Isometric bending of cylinders. (a) The theoretical prediction for the mean curvature (solid line) captures the numerical results for cylinders (blue symbols) as well as the numerical and experimental results (grey symbols) for the bending of bilayer plates from Pezzulla et al. (2016). (b) Energy profiles from theory (solid lines) and three-dimensional numerical simulations (symbols) for $h/R = (0.02, 0.04, 0.08)$. (c) Dimensionless snapping natural curvature from theory (solid line) and three-dimensional numerical simulations (symbols).

The first solution corresponds to the case in which the cylinders bend by keeping their generatrices orientated in the same direction, while the second solution corresponds to a rotated shape. By equating the two energies of the two solutions we find a critical *snapping* natural curvature that sets the threshold between the two

$$\bar{\kappa}_s = -\frac{1}{2R}, \quad (16)$$

which is independent of the Poisson ratio. These results may be expressed concisely in terms of the (dimensionless) mean curvature as

$$Hh = \frac{hf(\bar{\kappa})}{2\Lambda_o R} + \frac{1+\nu}{2}\bar{\kappa}h, \quad f(\bar{\kappa}) = \begin{cases} 1, & \bar{\kappa} > -\frac{1}{2R}, \\ \nu, & \bar{\kappa} < -\frac{1}{2R}. \end{cases} \quad (17)$$

Notice that when $R \rightarrow \infty$ the cylindrical shell becomes a flat plate and equation (17) converges to that presented in Pezzulla et al. (2016) except for a factor $1/\Lambda_o^2$, as given by equation (13) (with $\nu = 1/2$).

Figure 2 (a) shows the agreement of our theoretical prediction (17) with the numerical results for flat plates (from Pezzulla et al. (2016)) and cylinders (blue symbols), and experimental results (grey symbols) from Pezzulla et al. (2016) when $\nu = 1/2$. Notice how the *snapped* shapes obtained for $\bar{\kappa} < -1/(2R)$ are cylinders with generators rotated by 90 degrees with respect to the initial shape. Numerical simulations were performed to solve the geometrical problem within the context of finite (incompatible) tridimensional elasticity with large distortions using a Neo-Hookean incompressible material model (Lucantonio et al., 2014) implemented in the commercial software COMSOL Multiphysics. The shells were made of two layers: one layer was subjected to a distortion field $\mathbf{F}_o = \lambda(\mathbf{e}_1 \otimes \mathbf{e}_1 + \mathbf{e}_2 \otimes \mathbf{e}_2) + \mathbf{e}_3 \otimes \mathbf{e}_3$, whereas the other one was subjected to $\mathbf{F}_o = \mathbf{I}$. Then, the geometry was reduced to that of the beam, and we measured the curvature of the beam for each λ to determine $\bar{\kappa}$. Figure 2 (b) shows the energy profiles \bar{U}_b^1 (black line) and \bar{U}_b^2 (red line) as functions of $\bar{\kappa}$. Symbols represent energy profiles from three-dimensional numerical simulations that get closer to theoretical prediction for thinner shells. Notice also the emergence of a second minimum at zero energy, corresponding to a perfectly inverted and rotated cylinder, which becomes possible due to growth as the natural configuration continuously changes with $\bar{\kappa}$. Finally, figure 2 (c) shows the comparison between our theoretical prediction for the snapping natural curvature (solid line) and the numerical three-dimensional results.

4.3. Cones

Let us now consider a cone of length l with largest and smallest radius R_o and R_l , respectively. In this case the metric is still flat but non homogeneous. In cylindrical coordinates $(\eta^1, \eta^2) = (\theta, z)$, we have:

$$\bar{a}_{\alpha\beta} = \Lambda_o^2 \begin{pmatrix} R(z)^2 & 0 \\ 0 & 1 + c^2 \end{pmatrix}, \quad \bar{b}_\alpha^\eta = \begin{pmatrix} \frac{1}{\Lambda_o R(z) \sqrt{1+c^2}} + \bar{\kappa} & 0 \\ 0 & \bar{\kappa} \end{pmatrix}, \quad (18)$$

where $R(z) = cz + R_o$, with $c = (R_l - R_o)/l$. Again, we look for an isometric deformation of the cone by setting the stretching energy equal to zero. However, homogeneous second fundamental forms are not solutions of the Gauss-Codazzi-Mainardi equations:

$$\begin{aligned} b_{11,z} - b_{12,\theta} &= \frac{c}{R(z)} b_{11} + \frac{c}{1+c^2} R(z) b_{22}, \\ b_{12,z} - b_{22,\theta} &= -\frac{c}{R(z)} b_{12}, \\ b_{11} b_{22} - b_{12}^2 &= 0. \end{aligned} \quad (19)$$

The bending energy has to be minimized under these differential and algebraic constraints. This can be performed in COMSOL Multiphysics, in which we minimize the bending energy augmented by the three constraints imposed through three Lagrange multipliers fields. Moreover, we can assume that symmetry is preserved during the deformation so that $(\cdot)_{,\theta}$ and $b_{12} = b_{22} = 0$. Consequently, two of the original Gauss-Codazzi-Mainardi equations are trivially satisfied, while the other one can be solved analytically as

$$b_{11,z} = \frac{c}{cz + R_o} b_{11} \Rightarrow b_{11}(z) = A(cz + R_o), \quad A \in \mathbb{R}. \quad (20)$$

Substituting this solution in the bending energy density, this can be integrated to provide the bending energy up to the scalar parameter A . Therefore, the energy is now just a function that can be minimized with respect to A and the results may be expressed in terms of the dimensionless mean curvature as

$$H(z)h = \frac{h}{2(cz + R_o)} \left[\frac{1}{\Lambda_o \sqrt{1+c^2}} + \frac{(1+\nu)cl\bar{\kappa}}{\log(cl/R_o + 1)} \right]. \quad (21)$$

Note that for $c \rightarrow 0$, the cone approaches a cylinder of radius R_o , and, as expected, equation (21) approaches (17) for cylinders with $\bar{\kappa} > -1/(2R_o)$. Moreover, letting in addition $R \rightarrow \infty$, we recover the result for flat plates. The result for cones, equation (21), thus constitutes a generic result that holds for cones, cylinders, and plates. To make this more evident, we define

$$H_{\bar{\kappa}}(cl/R_o) := \partial_{\bar{\kappa}} H(z) \frac{cz + R_o}{R_o} = \frac{(1+\nu)cl/R_o}{2 \log(1 + cl/R_o)}, \quad (22)$$

which will prove to be useful to describe the influence of the slope of the cone on the deformed mean curvature. Notice indeed that for $c = 0$, $H_{\bar{\kappa}} = (1+\nu)/2$ that is exactly the first derivative of the mean curvature with respect to the natural curvature for plates and cylinders.

Figure 3 (left) shows the comparison among 3D numerical results (symbols), numerical constrained minimization (dashed red line) and analytical model (solid lines) in terms of the dimensionless mean curvature versus the longitudinal coordinate z/l for cones. As the natural curvature $\bar{\kappa}$ increases, the cone bends and both its two largest and smallest circles of radii R_o and R_l shrink, and the normalized mean curvature increases. While the analytical and constrained minimization models agree very well with each other, the 3D model shows the emergence of boundary layers that is a finite thickness effect. Figure 3 (right) shows how $H_{\bar{\kappa}}$ varies with cl/R_o according to the analytical prediction (solid line), numerical constrained minimization (dashed line) and 3D finite element model (symbols). The three cones above the plot correspond to $cl/R_o = -1, 0, 1$, from left to right: the cone corresponding to $cl/R_o = -1$ has a vertex at one end that is a pure tridimensional region of the body, completely ignored by our models. Indeed, while our analytical

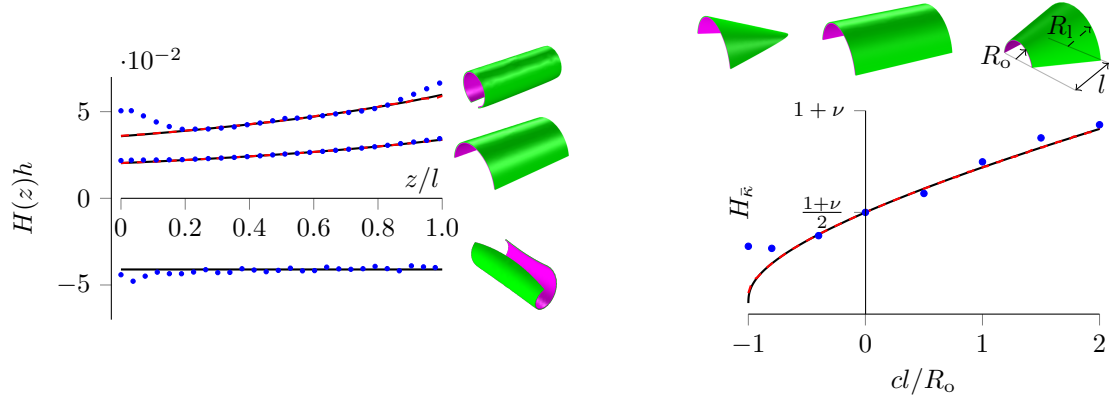


Figure 3: Isometric bending of cones. Dimensionless mean curvature as a function of z/l for three different values of natural curvature $\bar{\kappa}R_o = (0.07, 0.73, -1.43)$ and $cl/R_o = -0.4$ from the analytical model (solid line), numerical constrained minimization (dashed line) and 3D numerical results (symbols), and corresponding deformed shapes (left). Plot of $H_{\bar{\kappa}}$ versus cl/R_o from the analytical model (solid line), numerical constrained minimization (dashed line) and 3D numerical results (symbols). Three different cone geometries are shown for $cl/R_o = -1, 0, 1$, from left to right (right).

model predicts $H_{\bar{\kappa}} = 0$ (inconsistent with the geometry of the cone), the three-dimensional finite element results show a value greater than zero.

As investigated for cylindrical shells, we studied the snapping of conical shells triggered by a decreasing natural curvature and noticed a snapping transition where the orientation of the cone rotates by 90 degrees. Surprisingly, the resulting shape after snapping is very close to a cylinder for $|cl/R_o| < 1$, characterized by a roughly constant mean curvature along z , as indicated by 3D numerical results (symbols). Furthermore, we applied the formula for the morphing of cylinders having a radius equal to R_o (solid line), and found excellent agreement with numerics when $|cR_o/l| \ll 1$ (see *Appendix*).

5. Doubly curved shells

Finally, we investigate the growth of a spherical shell, which is both intrinsically and extrinsically curved. If we denote by R the radius of the shell, we have in spherical coordinates (u, v)

$$\bar{a}_{\alpha\beta} = \Lambda_o^2 \begin{pmatrix} R^2 & 0 \\ 0 & R^2 \sin^2 u \end{pmatrix}, \quad \bar{b}_{\alpha}^{\eta} = \begin{pmatrix} \frac{1}{\Lambda_o R} + \bar{\kappa} & 0 \\ 0 & \frac{1}{\Lambda_o R} + \bar{\kappa} \end{pmatrix}, \quad (23)$$

where $u \in [0, \theta]$ represents the colatitude of the shell (θ is called half-angle), while $v \in [0, 2\pi]$ is the azimuthal angle.

This configuration is analogous to the one that triggers harmomegathy in pollen grains (Katifori et al., 2010; Couturier et al., 2013). To test the model presented in Section 3, we start by a comparison between three-dimensional numerical results based on the model presented in Lucantonio et al. (2014), and a two-dimensional model based on C^1 -continuous subdivision finite elements (SDFEs) (Cirak and Ortiz, 2001). In the former, the outer layer of the shell swells while the inner layer shrinks, and we measure the corresponding natural curvature by running simulations of a beam; in the latter, equations (6) and (7) are directly implemented. As a consequence, if the two models show two shapes with equal deformation (and curvatures) for the same amount of natural curvature, the model presented in Section 3 is verified. In figure 4, we present the deformed shapes of spherical shells as obtained from the two-dimensional model (first row) and the three-dimensional model (second row) for different values of the half-angle $\theta = 45^\circ, 90^\circ, 135^\circ$; color code represents the dimensionless Gaussian curvature KR^2 . The models provide shapes that are in excellent agreement with each other, being the differences in the Gaussian curvature smaller than 1.4%. The boundary layer that develops along the edge clearly shows two peaks of the Gaussian curvature at two opposite locations.

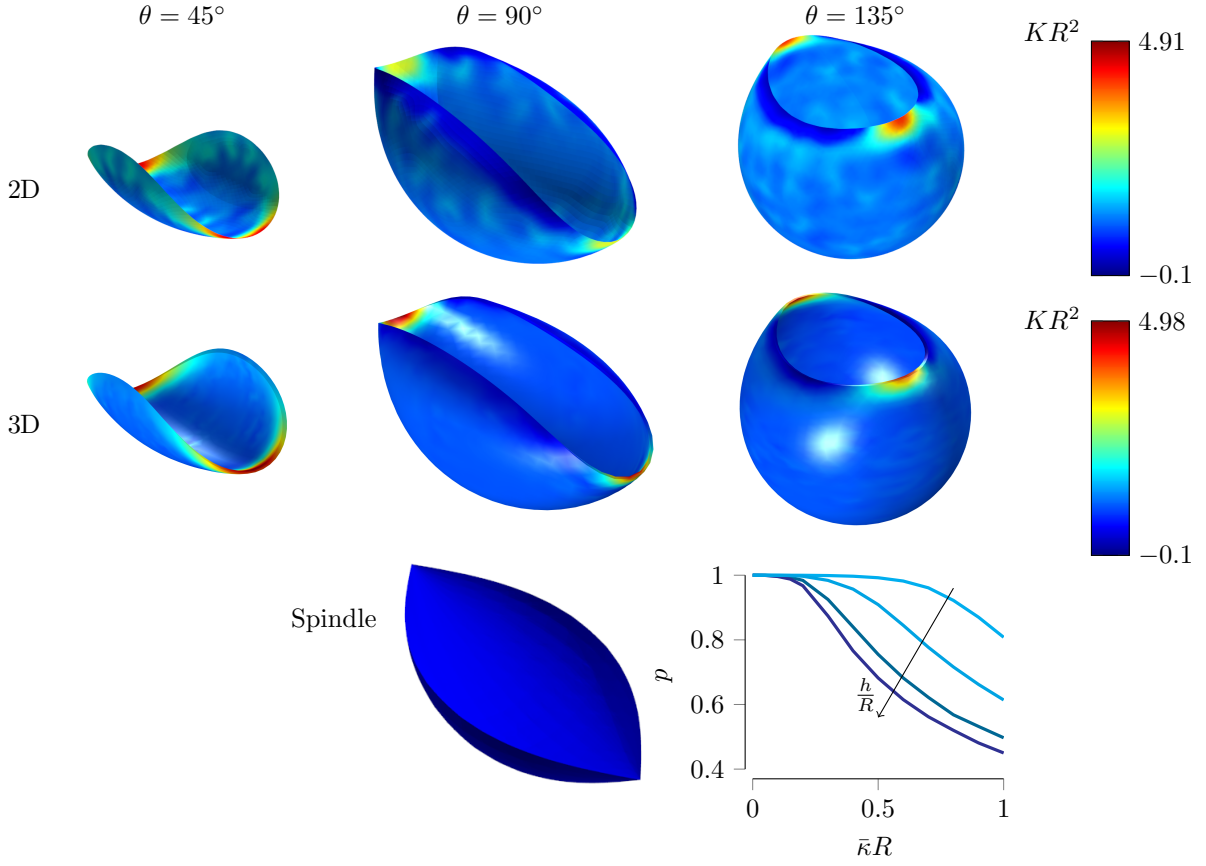


Figure 4: Nearly-isometric deformations of a spherical shell under increasing natural curvature. Comparison of the two-dimensional model (first row) and the three-dimensional model (second row) for three different half-angles, at $\bar{\kappa}R = 0.99$. In the third row, the spindle corresponding to the minimization of the bending energy when neglecting boundary layers of width $\sqrt{h/R}$ is shown. The plot shows the influence of the width of the boundary layer on the shape via the parameter p .

Contrary to the previous cases of cylinders and cones, there are no smooth surfaces that are isometric to a sphere (except any open subset of the sphere, which are of no interest for the problem at hand). A non smooth surface with homogenous positive Gaussian curvature is the spindle, and contains two vertices (singularities) at two opposite locations, exactly as the two peaks in the Gaussian curvature shown in the numerical results. A spindle can be parametrized (up to a scale factor) as a surface of revolution

$$\mathbf{r}(\eta^1, \eta^2) = (\Phi(\eta^2) \cos(\eta^1), \Phi(\eta^2) \sin(\eta^1), \Psi(\eta^2)), \quad (24)$$

where $\Phi(\eta^2) = p \cos(\eta^2)$ and $\Psi(\eta^2) = E(\eta^2 | p^2)$, where E denotes the incomplete elliptic integral of the second kind, and p is a parameter equals to 1 for a sphere and less than 1 for spindles: the smaller this parameter, the more elongated the shape of the spindle is. The Gaussian curvature is homogenous but singular at $\eta^2 = \pm\pi/2$ whereas the mean curvature is equal to

$$H(\eta^2) = \frac{(1 + p^2 \cos(2\eta^2)) \sec(\eta^2)}{2p\sqrt{1 - p^2 \sin^2(\eta^2)}}, \quad (25)$$

as well singular at $\eta^2 = \pm\pi/2$. The bending energy related to this configuration with respect to the natural forms (23) is then singular and diverges as

$$\bar{\mathcal{U}}_b \sim \frac{p^2 - 1}{2p} \log\left(\frac{\pi}{2} - \eta^2\right), \quad \text{as } \eta^2 \rightarrow \pi/2^-, \quad (26)$$

analogously to the divergence of the bending energy of e -cones (Müller et al., 2008). For $p = 1$, the spindle becomes a sphere and the singularities disappear. Therefore, the mapping (24) can be interpreted as a family

of deformations from a hemisphere to spindles. By neglecting an area around the two singularities with a magnitude comparable to the one of the boundary layer $\sqrt{h/R}$, the bending energy becomes finite and can be minimized with respect to p to give the shape in the last row of figure 4. Contrary to what shown for e cones in (Müller et al., 2008), the spindle that minimizes the bending energy does depend on the width of boundary layer neglected in the integration of the energy, as shown in the plot of figure 4. We note that there is no singularity apparent in the realized shape of the shell, as opposed to the presence of the vertex in an e -cone. The reasons for this difference could be rooted in the geometry of surfaces with singularities, as the spindle is an elliptic surface while the cone is parabolic, however, this question is beyond the scope of this work.

Finally, as for cylinders and cones, a negative natural curvature can trigger snap-through instabilities in spherical shells. A shell with an increasing natural curvature will then buckle in spindle-like shapes, whereas shells with decreasing natural curvature will snap. The competition between snapping and buckling of spherical shells will be addressed in a future work.

6. Conclusion

In this paper, we have derived a model for the growth of shells induced by variations in natural curvature starting from the theory of non-Euclidean plates. A three-dimensional, non-mechanical stimulus is reduced to the natural first and second fundamental forms of the mid-surface of the structure. The effect of the stimulus results to be additive to the initial geometric structure except for a spherical stretching factor that accounts for homotheties.

We have applied the model to different thin structures, from flat plates to spherical shells, finding excellent agreement between theory and numerics. As the results are derived from a purely geometrical model, they are applicable to a large variety of stimuli and, as such, are general and scalable.

Appendix A. Snapping and rotation for cones

Similarly to cylinders, cones can snap and rotate under a negative (decreasing) natural curvature. However, differently from cylinders, an isometric snapping and rotation is forbidden by geometrical compatibility conditions. Indeed, the Gauss-Codazzi-Mainardi equations (19) do not admit the snapped and rotated solution $b_{11} = b_{12} = 0$ and $b_{22} \neq 0$ since this implies

$$\frac{c}{1+c^2}R(z)b_{22} = 0. \quad (\text{A.1})$$

This means that when the cone snaps and rotates as observed in the numerical simulations, the mid-surface stretches. However, when $cl/R_o \ll 1$, the amount of stretch is small since equation (A.1) is satisfied at leading order. This explains why cones with small slopes snap and rotate very similarly to cylinders.

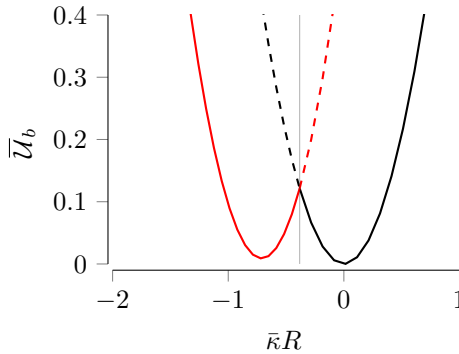


Figure A.5: Energy profiles for cone in the bending case (black line) and snapping/rotation case (red line).

To show why a rotated configuration is preferred for negative natural curvature also for conical geometries, we write the bending energy of cones:

$$\bar{U}_b = \int_{\omega} (1-\nu) \left[\left(\frac{A}{R(z)} - \left(\frac{1}{R(z)\sqrt{1+c^2}} + \bar{\kappa} \right) \right)^2 + (b_2^2 - \bar{\kappa})^2 \right] + \nu \left(\frac{A}{R(z)} - \frac{1}{R(z)\sqrt{1+c^2}} + b_2^2 - 2\bar{\kappa} \right)^2 d\omega, \quad (\text{A.2})$$

where we already used compatibility. This energy can be minimized with respect to A assuming $b_2^2 = 0$ to get equation (21). Similarly, when $cl/R_o \ll 1$, it can also be minimized with respect to b_2^2 assuming $A = 0$ to get

$$Hh = \frac{h}{2} \left[(1+\nu)\bar{\kappa} + \frac{\nu}{cl\sqrt{1+c^2}} \log \left(1 + \frac{cl}{R_o} \right) \right] = \frac{\nu h}{2R_o} + \frac{1+\nu}{2} \bar{\kappa} h + O(c), \quad (\text{A.3})$$

which is equal to the formula for the mean curvature of cylinders, at leading order. The energies corresponding to the two different solutions ($b_1^1 \neq 0$, $b_2^2 = 0$), equation (21), and ($b_1^1 = 0$, $b_2^2 \neq 0$), equation (A.3), can be plotted as functions of $\bar{\kappa}$ in figure A.5. The black solid line corresponds to ($b_1^1 \neq 0$, $b_2^2 = 0$) while the red line corresponds to ($b_1^1 = 0$, $b_2^2 \neq 0$). The behavior is similar to that encountered for cylinders although is more complicated, and approximately valid only for $cl/R_o \ll 1$. The critical value of the natural curvature is a function of the Poisson ratio in this case, and the geometry of the cone, while the second minimum of the bending energy is not a zero energy state.

Acknowledgments

D.P.H. is grateful for financial support from the NSF CAREER CMMI-1454153.

References

- Amar, M.B., Goriely, A., 2005. Growth and instability in elastic tissues. *Journal of the Mechanics and Physics of Solids* 53, 2284–2319. doi:10.1016/j.jmps.2005.04.008.
- Armon, S., Efrati, E., Kupferman, R., Sharon, E., 2011. Geometry and mechanics in the opening of chiral seed pods. *Science* 333, 1726–1730. URL: <http://www.sciencemag.org/content/333/6050/1726.abstract>, doi:10.1126/science.1203874, arXiv:<http://www.sciencemag.org/content/333/6050/1726.full.pdf>.
- Audoly, B., Pomeau, Y., 2010. *Elasticity and Geometry: From Hair Curls to the Non-linear Response of Shells*. OUP Oxford. URL: <https://books.google.com/books?id=FMQRDAAAQBAJ>.
- Boudaoud, A., 2010. An introduction to the mechanics of morphogenesis for plant biologists. *Trends in Plant Science* 15, 353–360. URL: <http://www.sciencedirect.com/science/article/pii/S1360138510000701>.
- Charlet, P., 2000. *Theory of Shells. Mathematical Elasticity*, Elsevier Science. URL: https://books.google.fr/books?id=EYAxQ77o_6QC.
- Cirak, F., Ortiz, M., 2001. Fully c1-conforming subdivision elements for finite deformation thin-shell analysis. *International Journal for Numerical Methods in Engineering* 51, 813–833. URL: <http://dx.doi.org/10.1002/nme.182>, doi:10.1002/nme.182.
- Couturier, E., Dumais, J., Cerda, E., Katifori, E., 2013. Folding of an opened spherical shell. *Soft Matter* 9, 8359–8367. URL: <http://dx.doi.org/10.1039/C3SM50575H>, doi:10.1039/C3SM50575H.
- Efrati, E., Sharon, E., Kupferman, R., 2009. Elastic theory of unconstrained non-euclidean plates. *J. Mech. Phys. Solids* 57, 762 – 775. URL: <http://www.sciencedirect.com/science/article/pii/S0022509608002160>, doi:<http://dx.doi.org/10.1016/j.jmps.2008.12.004>.
- Efrati, E., Sharon, E., Kupferman, R., 2010. Non-euclidean plates and shells URL: <https://web.archive.org/web/20161107213906/http://math.huji.ac.il/~razk/Publications/PDF/ESK09b.pdf>.
- Goriely, A., Ben Amar, M., 2005. Differential growth and instability in elastic shells. *Phys. Rev. Lett.* 94, 198103. URL: <http://link.aps.org/doi/10.1103/PhysRevLett.94.198103>, doi:10.1103/PhysRevLett.94.198103.
- Höhn, S., Honerkamp-Smith, A.R., Haas, P.A., Trong, P.K., Goldstein, R.E., 2015. Dynamics of a *Volvox* embryo turning itself inside out. *Phys. Rev. Lett.* 114, 178101. URL: <http://link.aps.org/doi/10.1103/PhysRevLett.114.178101>, doi:10.1103/PhysRevLett.114.178101.
- Holmes, D.P., Roché, M., Sinha, T., Stone, H.A., 2011. Bending and twisting of soft materials by non-homogenous swelling. *Soft Matter* 7, 5188–5193. doi:10.1039/C0SM01492C.
- Hong, W., Zhao, X., Zhou, J., Suo, Z., 2008. A theory of coupled diffusion and large deformation in polymeric gels. *Journal of the Mechanics and Physics of Solids* 56, 1779 – 1793. URL: <http://www.sciencedirect.com/science/article/pii/S0022509607002244>, doi:<http://dx.doi.org/10.1016/j.jmps.2007.11.010>.
- von Kármán, T., 1910. Festigkeitsprobleme im maschinenbau. *Encyklopädie der Mathematischen Wissenschaften* 4, 311–385.
- Katifori, E., Alben, S., Cerda, E., Nelson, D.R., Dumais, J., 2010. Foldable structures and the natural design of pollen grains. *Proceedings of the National Academy of Sciences* 107, 7635–7639. doi:10.1073/pnas.0911223107.

- Kebadze, E., Guest, S., Pellegrino, S., 2004. Bistable prestressed shell structures. *International Journal of Solids and Structures* 41, 2801–2820. URL: <http://www.sciencedirect.com/science/article/pii/S0020768304000460>, doi:<http://dx.doi.org/10.1016/j.ijsolstr.2004.01.028>.
- Kim, J., Hanna, J.a., Byun, M., Santangelo, C.D., Hayward, R.C., 2012. Designing responsive buckled surfaces by halftone gel lithography. *Science* 335, 1201–1205. URL: <http://www.ncbi.nlm.nih.gov/pubmed/22403385>, doi:10.1126/science.1215309.
- Klein, Y., Efrati, E., Sharon, E., 2007. Shaping of elastic sheets by prescription of non-euclidean metrics. *Science* 315, 1116–1120. URL: <http://science.sciencemag.org/content/315/5815/1116>, doi:10.1126/science.1135994, arXiv:<http://science.sciencemag.org/content/315/5815/1116.full.pdf>.
- Klein, Y., Venkataramani, S., Sharon, E., 2011. Experimental study of shape transitions and energy scaling in thin non-euclidean plates. *Phys. Rev. Lett.* 106, 118303. URL: <http://link.aps.org/doi/10.1103/PhysRevLett.106.118303>, doi:10.1103/PhysRevLett.106.118303.
- Koiter, W.T., Simmonds, J.G., 1973. *Foundations of shell theory*. Springer Berlin Heidelberg, Berlin, Heidelberg. pp. 150–176. URL: http://dx.doi.org/10.1007/978-3-642-65590-6_11, doi:10.1007/978-3-642-65590-6_11.
- Kondaurov, V., Nikitin, L., 1987. Finite strains of viscoelastic muscle tissue. *Journal of Applied Mathematics and Mechanics* 51, 346–353. URL: <http://www.sciencedirect.com/science/article/pii/0021892887901110>, doi:[http://dx.doi.org/10.1016/0021-8928\(87\)90111-0](http://dx.doi.org/10.1016/0021-8928(87)90111-0).
- Lewicka, M., 2011. *Reduced Theories in Nonlinear Elasticity*. Springer US, Boston, MA. pp. 393–403. URL: http://dx.doi.org/10.1007/978-1-4419-9554-4_22, doi:10.1007/978-1-4419-9554-4_22.
- Love, A.E.H., 1888. The small free vibrations and deformation of a thin elastic shell. *Philosophical Transactions of the Royal Society of London A: Mathematical, Physical and Engineering Sciences* 179, 491–546. URL: <http://rsta.royalsocietypublishing.org/content/179/491>, doi:10.1098/rsta.1888.0016, arXiv:<http://rsta.royalsocietypublishing.org/content/179/491.full.pdf>.
- Lucantonio, A., Nardinocchi, P., Pezzulla, M., Teresi, L., 2014. Multiphysics of bio-hybrid systems: shapecontrol and electro-induced motion. *Smart Materials and Structures* 23, 045043. URL: <http://stacks.iop.org/0964-1726/23/i=4/a=045043>.
- Lucantonio, A., Nardinocchi, P., Teresi, L., 2013. Transient analysis of swelling-induced large deformations in polymer gels. *Journal of the Mechanics and Physics of Solids* 61, 205–218. URL: <http://www.sciencedirect.com/science/article/pii/S0022509612001548>, doi:<http://dx.doi.org/10.1016/j.jmps.2012.07.010>.
- Lucantonio, A., Tomassetti, G., DeSimone, A., 2016. Large-strain poroelastic plate theory for polymer gels with applications to swelling-induced morphing of composite plates. *Composites Part B: Engineering*, –URL: <http://www.sciencedirect.com/science/article/pii/S1359836816320406>, doi:<http://dx.doi.org/10.1016/j.compositesb.2016.09.063>.
- Moshe, M., Sharon, E., Kupferman, R., 2013. Pattern selection and multiscale behaviour in metrically discontinuous non-euclidean plates. *Nonlinearity* 26, 3247. URL: <http://stacks.iop.org/0951-7715/26/i=12/a=3247>.
- Müller, M.M., Amar, M.B., Guven, J., 2008. Conical defects in growing sheets. *Phys. Rev. Lett.* 101, 156104. URL: <http://link.aps.org/doi/10.1103/PhysRevLett.101.156104>, doi:10.1103/PhysRevLett.101.156104.
- Nardinocchi, P., Teresi, L., 2007. On the active response of soft living tissues. *Journal of Elasticity* 88, 27–39. URL: <http://dx.doi.org/10.1007/s10659-007-9111-7>.
- O’Neill, B., 1997. *Elementary Differential Geometry*. Academic Press. URL: <https://books.google.fr/books?id=4uMAw3NwnmgC>.
- Pezzulla, M., Shillig, S.A., Nardinocchi, P., Holmes, D.P., 2015. Morphing of geometric composites via residual swelling. *Soft Matter* 11, 5812–5820. URL: <http://dx.doi.org/10.1039/C5SM00863H>, doi:10.1039/C5SM00863H.
- Pezzulla, M., Smith, G.P., Nardinocchi, P., Holmes, D.P., 2016. Geometry and mechanics of thin growing bilayers. *Soft Matter* 12, 4435–4442. URL: <http://dx.doi.org/10.1039/C6SM00246C>, doi:10.1039/C6SM00246C.
- Py, C., Reverdy, P., Doppler, L., Bico, J., Roman, B., Baroud, C.N., 2007. Capillary origami: Spontaneous wrapping of a droplet with an elastic sheet. *Phys. Rev. Lett.* 98, 156103. URL: <http://link.aps.org/doi/10.1103/PhysRevLett.98.156103>, doi:10.1103/PhysRevLett.98.156103.
- Rayleigh, J., 1894. *The Theory of Sound*. Number v. 1 in *The Theory of Sound*, Macmillan. URL: <https://books.google.com/books?id=hd8EAAAAYAAJ>.
- Sadik, S., Angoshtari, A., Goriely, A., Yavari, A., 2016. A geometric theory of nonlinear morphoelastic shells. *Journal of Nonlinear Science* 26, 929–978. URL: <http://dx.doi.org/10.1007/s00332-016-9294-9>, doi:10.1007/s00332-016-9294-9.
- Timoshenko, S., 1925. Analysis of bi-metal thermostats. *J. Opt. Soc. Am.* 11, 233–255. URL: <http://www.opticsinfobase.org/abstract.cfm?URI=josa-11-3-233>, doi:10.1364/JOSA.11.000233.